Zonal flow triggers the L-H transition in the Experimental Advanced Superconducting Tokamak

P. Manz,[1,2] G. S. Xu,[3] B. N. Wan,[3] H. Q. Wang,[3] H. Y. Guo,[3] I. Cziegler,[1,2] N. Fedorczak,[1,2] C. Holland,[2] S. H. Müller,[1,2] S. C. Thakur,[1,2] M. Xu,[1,2] K. Miki,[4] P. H. Diamond,[1,4,5] and G. R. Tynan[1,2]

[1]*Center for Momentum Transport and Flow Organization, University of California at San Diego, San Diego, California 92093, USA*
[2]*Center for Energy Research, University of California at San Diego, San Diego, California 92093, USA*
[3]*Institute of Plasma Physics, Chinese Academy of Sciences, Hefei 230031, China*
[4]*WCI Center for Fusion Theory, National Fusion Research Institute, Gwahangno 113, Yusung-gu, Daejeon 305-333, Korea*
[5]*Center for Astrophysics and Space Science & Department of Physics, University of California at San Diego, California 92093, USA*

(Received 31 May 2012; accepted 22 June 2012; published online 23 July 2012)

The kinetic energy transfer between shear flows and the ambient turbulence is investigated in the Experimental Advanced Superconducting Tokamak during the L-H transition. As the rate of energy transfer from the turbulence into the shear flow becomes comparable to the energy input rate into the turbulence, the transition into the H-mode occurs. As the observed behavior exhibits several predicted features of zonal flows, the results show the key role that zonal flows play in mediating the transition into H-mode. © *2012 American Institute of Physics*. [http://dx.doi.org/10.1063/1.4737612]

INTRODUCTION

The transition from low (*L*-mode) to high confinement (*H*-mode) regime in magnetized confined fusion devices occurs very rapidly at a critical condition, similar, in a sense, to leaning slightly over the side of a canoe causing only a small tilt of the craft, but leaning slightly more may roll you and the craft into the lake. Rapid threshold transitions between distinctly different stable states then require a triggering event, akin to leaning out too far from the canoe.[1] However, the physics that triggers the transition into *H*-mode is not understood, and thus predictions of the conditions for the transition into the *H*-mode regime—which are critical for the operation of ITER in the burning plasma regime—are based on empirical scalings with a wide range of uncertainty. Relative to the conditions found in low confinement regimes, *H*-mode plasmas are characterized by a reduced turbulence level and strong radial electric field (E_r) shear.[2,3] Azimuthally symmetric, bandlike, time-varying, turbulent generated shear flows called zonal flows (ZFs) also appear to be associated with the *L–H* transition.[4,5] Therefore, the interaction between micro and macroscale turbulent fluctuations has developed into one of the most active research topics in the physics of magnetized plasmas. The main focus has been placed on the generation of zonal flows and the reduction of the ambient turbulence via the nonlinear exchange, or transfer, of energy from the smaller scaled higher frequency turbulent fluctuations into the large scale, low frequency ordered zonal flow.[6–14]

SELF-REGULATION OF TURBULENCE

Theory predicts that the *L–H* transition can be explained by an intermediate, quasi-periodic transient stage, where turbulence, zonal flow, mean shear flow, and the pressure gradient are coupled.[15,16] In this model, as the input power increases the pressure gradient also increases, resulting in stronger instabilities and fluctuation levels. The turbulence level grows and begins to nonlinearly drives the zonal flow until the zonal flow drive can overcome the flow damping. A finite zonal flow then begins to grow and extract kinetic energy from the turbulence and thereby acts to suppress the turbulence amplitude. Zonal flows can trigger the transition by regulating the turbulence level and associated transport until the mean shear flow is high enough to suppress the remaining turbulence and associated transport, causing the pressure gradient to increase by radial force balance. As a result, the mean radial electric field shear increases to the point where it can maintain a state of suppressed turbulence. In the absence of a turbulent drive, the zonal flow then dies away. For input powers just below the transition threshold, self-regulation between turbulence and zonal flows occur as an oscillatory behavior, characteristic of predator-prey systems. Recently, these predator-prey oscillations have been observed in various devices.[17–21] For a faster heat power ramp, a classic *L–H* transition can occur, characterized by a single burst of zonal flow energy that extracts the most or all of the energy from the turbulence. This is followed by the collapse of the turbulence and onset of a strong radial electric field shear sustained by the ion pressure gradient.[22]

Up to now, all experimental investigations of energetic interaction between zonal flows and the ambient turbulence studied the temporal relationship between turbulence amplitudes, zonal flow amplitudes, and the evolution of the sheared background mean radial electric field; the results of these studies have been qualitatively consistent with the predator-prey model. However, an essential piece of the physics—namely, the nonlinear exchange of energy between the turbulence (the prey) and the zonal flow (the first

predator) in the presence of a background mean sheared $E \times B$ flow (second predator) has to date never been studied during the *L–H* transition. In this work, we perform the first such study by inserting a suitably arranged Langmuir probe array inside the separatrix region of a discharge which undergoes an *L–H* transition, and thereby providing the first quantitative measurement of the energetics of turbulence-zonal flow coupling during the *L–H* transition.

In order to motivate the data analysis strategy, it is useful to write a schematic set of coupled predator-prey equations for the zonal flow—drift-wave system. These are

$$\frac{\partial}{\partial t}\epsilon_T = \gamma_{eff}\epsilon_T - \langle \tilde{v}_r \tilde{v}_\theta \rangle \frac{\partial v_{ZF}}{\partial r}, \tag{1a}$$

$$\frac{\partial}{\partial t}\epsilon_{ZF} = \langle \tilde{v}_r \tilde{v}_\theta \rangle \frac{\partial v_{ZF}}{\partial r} - \mu \epsilon_{ZF}. \tag{1b}$$

Here, $\epsilon_T = \langle \tilde{v}^2 \rangle$ and $\epsilon_{ZF} = \langle v_{ZF} \rangle^2$ are the turbulence and zonal flow energies, respectively, and γ_{eff} is a total, effective growth rate, including gradient drive, mean shearing, and nonlinear mixing. Thus, $\gamma_{eff} = \gamma_{eff}(\nabla T, \nabla n, \langle v_E^{'} \rangle, \epsilon_T, \ldots)$ and is measured experimentally by study of fluctuation recovery rates γ_{eff} during the limit cycle regime occurring at the power threshold. Of course,

$$\mathcal{P}_\perp = \langle \tilde{v}_r \tilde{v}_\theta \rangle \frac{\partial \langle v_{ZF} \rangle}{\partial r} \tag{2}$$

is the Reynolds work of the fluctuations on the flow. $\langle \tilde{v}_r \tilde{v}_\theta \rangle \sim \pm \partial v_{ZF}/\partial r$ indicates negative (i.e., zonal flow growth) or positive (i.e., zonal flow damping) viscosity, respectively. This Reynolds work term is usually measured by bicoherence studies.[6,8–13,23] However, bispectral analysis needs long stationary time series, which are generally not available in high temperature fusion plasmas. Furthermore, the *L–H* transition is inherently non-stationary. Therefore, to estimate the energy transfer between the shear flow and the turbulence, we use an approach similar to that of Refs. 24 and 25 in which the relevant quantities are computed in the time-domain using suitably filtered and averaged quantities. Here, μ is the total zonal flow damping rate, including collisional, charge exchange, and nonlinear damping. We do not present a direct measurement of μ in this paper, but this might be approached by studying the decay rate of the zonal flow energy in the *H*-mode, when turbulence damping eliminates the Reynolds work source in the ϵ_{ZF} Eq. (1b).

The obvious criterion for triggering of the *L–H* transition is $\partial \epsilon_T/\partial t < 0$, with a positive phase between $\langle \tilde{v}_r \tilde{v}_\theta \rangle$ and $\partial v_{ZF}/\partial r$—i.e., negative viscosity which results in a net decay of the fluctuation energy. In this case, the zonal flow is sinking energy from the turbulence faster than the turbulence grows. This requires

$$\frac{\langle \tilde{v}_r \tilde{v}_\theta \rangle \frac{\partial \langle v_{ZF} \rangle}{\partial r}}{\gamma_{eff}\epsilon_T} > 1, \tag{3}$$

which emerges as a natural figure of merit for the collapse of the turbulence and the onset of transition. In terms of experimentally measurable quantities, Eq. (3) requires that the turbulence-to-zonal flow energy transfer $\mathcal{P}_\perp$ exceed the change in turbulence intensity during a recovery period, i.e., $\mathcal{P}_\perp/\gamma_{eff}\langle \tilde{v}^2 \rangle > 1$. This condition then defines a criterion which the normalized energy transfer must satisfy. Thus, a suitably arranged experiment can measure the appropriate quantities to test this model of the *L–H* transition.

EXPERIMENTAL SETUP

Such an experiment has been carried out on the Experimental Advanced Superconducting Tokamak (EAST) ($R_0 = 1.88$ m, $a = 0.45$ m, $B_t = 1.4-2$ T, $I_p = 0.4-0.8$ MA), where the *H*-mode has been achieved by lower hybrid wave current drive with the total heating power limited to about 1 MW.[26] Floating potential fluctuations interpreted as plasma potential fluctuations are measured with a Langmuir probe array[11,27] consisting of three tips. Two tips are poloidally separated by 8 mm, a third tip is placed in the middle of them, radially sticking out by 5 mm. This configuration allows an estimate of the Reynolds stress as done in Ref. 20. The probe array has been inserted ~1.5 cm inside the separatrix as estimated by observing a break in the slope of the DC floating potential profile and also by estimating the separatrix position from reconstructions of the MHD equilibrium. Data are taken at a sampling rate of 5 MHz.

EXPERIMENTAL RESULTS

The discharge (shot 36030) shown in red is that of Ref. 20. For comparison, also a discharge (shot 36071) at similar plasma parameters is included in blue in the figures. Figure 1 shows some basic features of the discharge. A representative limit cycle oscillation in the floating potential is depicted in Fig. 1(a). Fig. 1(b) shows 2 seconds of data and illustrates two transitions—the first is a classic *L–H* transition at 3521.5 ms, which is analyzed here, while the second, documented by the second probe plunge, is a dithering phase at 4300–4350 ms exhibiting multiple limit cycle orbits and has been reported in detail in Ref. 20. A zonal flow has been identified as a coherent mode at 2 kHz, which is driven by broadband turbulent fluctuations between 30 and 100 kHz.[20] The scale separation of the relevant quantities is necessary to extract their energy transfer by Eq. (2) which through the time-averaging operation requires the identification of the turbulent scales and (separately) the zonal flow scale. The vertical extreme ultraviolet (XUV) emission profiles, proportional to plasma density and electron temperature, are nearly identical for these two transitions (Fig. 1(d)), indicating that the time average gradients at the plasma edge are about the same in the two transitions. Thus, the turbulence recovery rate as an approximate measure of the effective growth rate γ_{eff} during the dithering phase is appropriate to investigate the first *L–H* transition. A histogram of the energy recovery time, $1/\gamma_{eff}$, estimated from 27 limit cycle oscillations in the dithering phase is shown in Fig. 1(c), along with a smoothed probability density function (PDF) computed from these data. From this result, we find that the average turbulent energy recovery time is approximately 90 μs. The net power input into the turbulence, which varies in proportion to the turbulent kinetic energy during the transition, is then given by $\gamma_{eff}\tilde{v}_\perp^2$.

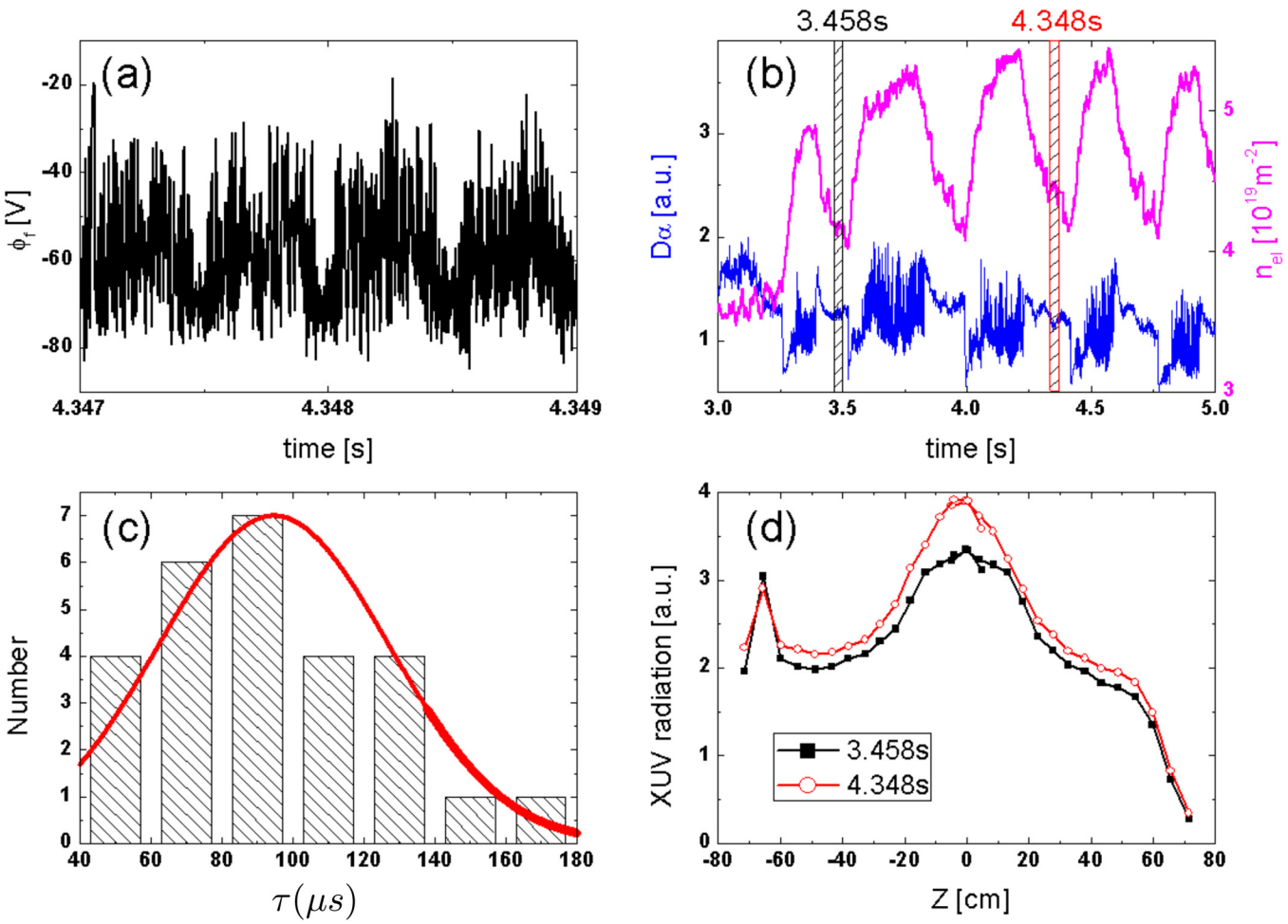

FIG. 1. (a) A representative limit cycle oscillation in the floating potential, (b) D_α and density, (c) PDF of the energy recovery time, and (d) XUV radiation.

Consistent with the observed frequencies for turbulent and flow scales, the Reynolds stress during the *L–H* transition is calculated from high pass ($f > 15$ kHz) filtered floating potential fluctuations and the sheared flow from low pass ($f < 2$ kHz) filtered floating potential fluctuations, which are then used to estimate the electric field and $E \times B$ drift motion. This scale separation is consistent with the previously identified regimes of turbulence and zonal flow in the EAST device;[20] however, we note that the results discussed below are not sensitive to the precise choice of these frequency bands and thus do not change the conclusions arising from the analysis. Measurements show that the poloidal velocity at the separatrix is small compared to the values at 1.5 cm inside. We thus take the poloidal velocity at the separatrix to be zero and calculate $\partial_r \langle v_\theta \rangle \approx -\langle v_\theta \rangle / \Delta r$, with $\Delta r = 1.5$ cm be the distance to the separatrix, allowing us to then estimate $\mathcal{P}_\perp \approx \langle \tilde{v}_r \tilde{v}_\theta \rangle \langle v_\theta \rangle / \Delta r$. It is unlikely that the probe is any deeper than 1.5 cm inside the last closed flux surface (LCFS) (otherwise, it would overheat and inject large quantities of impurities into the plasma). Therefore, the estimated production values (shown in Figs. 2(d) and 2(e)) likely represent minima; actual production rates could be higher by as much as a factor of 2-3 determined mostly by uncertainties in the depth of probe penetration.

Figure 2 shows the time traces of the D_α signal indicating an *L–H* transition. Here, we have set $t = 0$ to correspond to the beginning of the drop in D_α for all of the discharges shown. To guide the eye, the *L–H* transition is indicated by a gray box. The relation between the energy in the shear flow and the turbulence can also be represented by a hodograph as shown in Fig. 3 similar to that of Ref. 18. In Figures 2 and 3, we define several key periods in the transition as phase (I), phase (II), and phase (III). The evolution of the kinetic energy in the turbulence and low frequency flow across this transition are shown in Figs. 2(b) and 2(c). The results show that 3 ms before the *L–H* transition, the turbulent fluctuation amplitude (Fig. 2(b)) increases defining phase (I) of the transition. At about 1 ms before the *L–H* transition, the kinetic energy in the low frequency flow (Fig. 2(c)) builds up and the energy in the higher frequency fluctuations (Fig. 2(b)) drops, defining phase (II) of the transition. The growth of the flow appears on the fast, turbulent time scales (i.e., 100's of μs) providing a strong indication that the flow is turbulence generated, and therefore a zonal flow. We observe a small phase lag between flow and turbulent energy (Figs. 2(b) and 2(c)) consistent with the predator (zonal flow) following the prey (turbulence) in time. Once the shear flow grows to large enough amplitude, the turbulence induced flow shear then causes a reduction in the turbulent amplitude and the flow

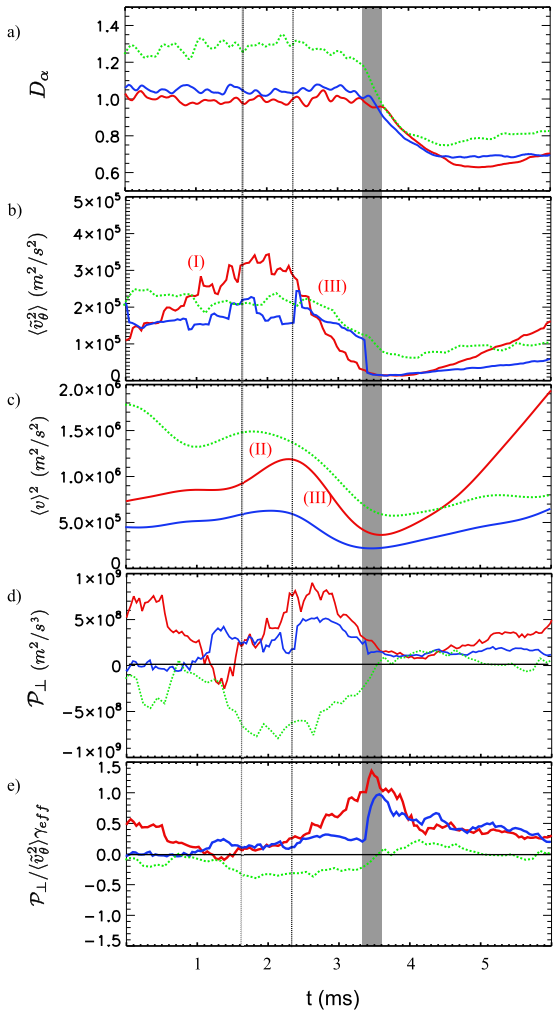

FIG. 2. D_α (a), turbulent (b), and flow (c) fluctuation amplitude during *L–H* transition. Energy transfer between turbulence and shear flow (d) and normalized to turbulent fluctuation amplitude and energy recovery time (e). Data from 1.0–1.5 cm inside LCFS denoted by blue and red curves. Data taken 1 cm outside of LCFS in the SOL region denoted by green curve.

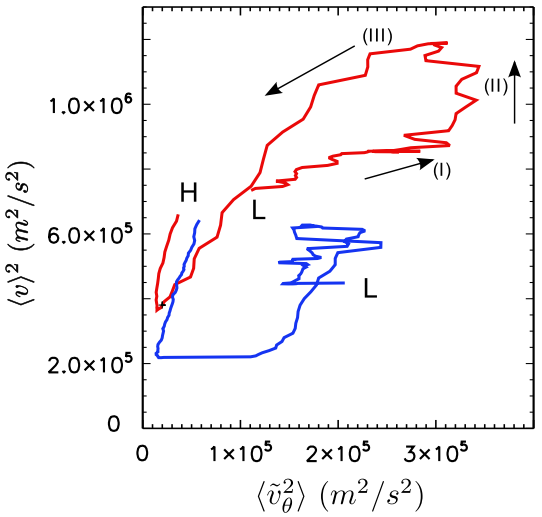

FIG. 3. Hodograph of turbulent and flow energies during L-H transition.

then begins to decay, defining phase (III) in the transition, consistent with recent observations in TJ-II.[18] The delay between the reduction in the turbulent amplitude and the drop of the D_α (Figs. 2(a) and 2(b)) most likely corresponds to a combination of the time needed for cross-field transport and parallel flow from the midplane region to the divertor region where the D_α emissions are observed. The kinetic energy transfer $\mathcal{P}_\perp$ from the turbulence into the shear flow continues to increase while the turbulence amplitude is decreasing (Fig. 2(d)) during phase (III), while the *L–H* transition is approached as shown in Fig. 2(d)). This confirmed the earlier conjecture above that the low frequency flow is actually driven by a transfer of energy from the turbulence. About 1 ms before the *L–H* transition occurs, the kinetic energy transfer $\mathcal{P}_\perp$ peaks. To evaluate whether this energy transfer is sufficient to reduce the turbulence level significantly the transfer rate must be compared to the energy input rate into the turbulence as discussed above. Using experimental data, we find the ratio of the production, $\mathcal{P}_\perp$, normalized by $\gamma_{eff} \langle \tilde{v}_\perp^2 \rangle$ in Figure 2(e). This ratio indicates the power transfer rate into the shear flow normalized by the power transfer into the turbulence from the combined effects of the free energy source and the background E_r shearing during periods of weak flow. As the D_α signal starts to drop (the traditional measure of the start of the *L–H* transition), the turbulence has already reached its minimum. Commensurate with the drop in D_α signal, the flow production rate surpasses the turbulence recovery rate and the turbulence energy collapses to nearly zero. After the peak of the normalized production rate, the production $\mathcal{P}_\perp$ remains small and the low. But the low frequency flow begins to recover (Fig. 2(c)), suggesting that after the transition the flow is sustained by non-turbulent processes. The growth of the radial electric field and associated flow shear after the drop in D_α light has already been shown to be associated with the growth of the ion pressure gradient.[28] No ion temperature profiles are available here, but the observation here is consistent with this earlier result. Furthermore, in an analysis of similar data obtained just outside of the separatrix (shown in green in Fig. 2), no such transient behavior is observed. This indicates that these observations are isolated to the region inside the LCFS, and that on open field lines the turbulence amplitude simply collapses after the *H*-mode transition, as has been reported earlier.[3]

COMPARISON WITH PRESENT PREDATOR-PREY MODEL

The one-space, one-time multiple shearing predator-prey model[22] is used for comparison with the experimental results reported here from EAST. A fast ramp of the heating power is used to model the regular *L–H* transition. Under these conditions, no limit-cycle oscillation is observed. Instead, a single burst of zonal flow energy and turbulence collapse is observed, followed by a classic *L–H* transition. A typical time trace around the *L–H* transition is shown in Fig. 4. Here, Fig. 4(a) depicts the evolution of the amplitudes of the turbulence I, the zonal flow E_0^2, and the mean flow. The modest decrease of turbulence I in the early part of the model evolution is triggered by a rapid growth of the mean flow, or a decorrelation of turbulence drive by mean flow shearing. The coupling between the zonal flow and the turbulence is

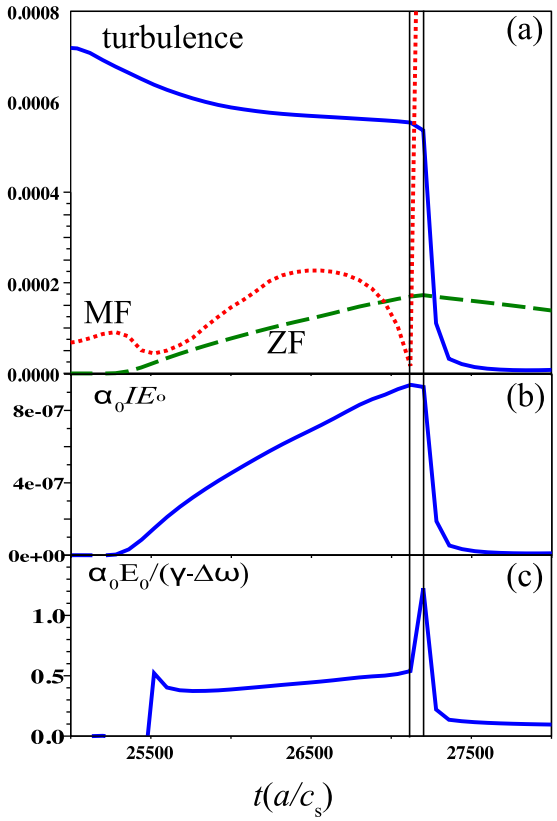

FIG. 4. Predator-prey model with fast power ramp up. Evolution of the turbulent, ZF, and mean flow (MF) amplitudes (a), the zero frequency ZF shearing (b), and normalized energy transfer (c). Model is described in detail in Ref. 22.

given by $\alpha_0 IE_0^2$, where α_0 is the coupling parameter between them. As seen in Fig. 4(b), the coupling increases toward the *L–H* transition. A small increase of zonal flow and a decrease of turbulence lead to a large peak in the production rate, normalized to the net energy input rate (Fig. 4(c)). This peak is a trigger of a rapid quench of turbulence, i.e., the *L–H* transition. Comparing the experimentally observed normalized energy production $\mathcal{P}_\perp/\gamma_{eff}\tilde{v}_\perp^2$ to the results in Figure 4(c), we observe a very similar peaking in the normalized energy production rate in both experiment and model.

DISCUSSION

Obtaining these type of probe data—which provide the key physics data needed to test the role of turbulence-zonal flow coupling in the *L–H* transition—are technically challenging and thus at present data from only a few discharges are available. Taken in isolation, such observations would not be sufficient to make a firm claim that the role of the zonal flow as a trigger mechanism for the *L–H* transition has been conclusively demonstrated. However, the results reported here cannot be viewed in isolation, but rather must be seen as building on the substantial body of evidence that turbulence-driven zonal flows or geodesic acoustic modes play an important role in triggering the *L–H* transition. For example, the observed transient shear flow just prior to the *L–H* transition certainly exhibits several features that are consistent with it being a zonal flow. In particular, it shows a strong bicoherence and Reynolds stress modulation indicating the nonlinear drive by the turbulence, features a toroidal mode number of zero, and exhibits the characteristic predator-prey oscillations.[20] These features have been observed not only in EAST (Ref. 20) but have been observed in other devices.[17,18,21] The limit-cycle behavior between the radial electric field and the turbulent amplitude just prior to the *L–H* transition has been shown also in TJ-II.[18] Afterward, ASDEX-U[17] and DIII-D[21] have investigated these limit-cycles in detail documenting the existence of an intermediate phase between *L* and *H* mode, called *I* phase. Both devices report strong oscillations in the shearing rates in this regime showing the importance of time-varying shear flows during the limit-cycles. Where ASDEX-U reported geodesic acoustic modes responsible for the limit-cycle behavior,[17] the work on DIII-D points to low frequency zonal flows.[21] However, both emphasize the importance of turbulent generated shear flows. Finally, we note that studies of the transition to a state of improved Ohmic confinement in HT-7[29] show a transient increase in the turbulent Reynolds stress and the sheared poloidal $E \times B$ flow just before the confinement transition, consistent with the development of a turbulence-driven zonal flow just prior to the development of the improved confinement regime. Work in DIII-D during a normal *L–H* transition in an auxiliary heated discharge showed a few ms long transient increase between the broadband turbulence and a low-frequency potential fluctuation just inside the LCFS.[23] The new evidence reported here builds on these earlier results by investigating the physics of the trigger mechanism directly, by estimating the suppression strength due to the generation of these shear flows and compares the generation rate of the shear flows to the energy input rate from the free energy source. Our estimation (even though rough, but novel) shows that the zonal flow is strong enough to suppress the turbulence over a time sufficient that the transition into the *H*-mode occurs. A comparison with the predator-prey model is then able to reproduce these essential features. Talking together all these observations in different devices with different diagnostics and the good agreement with present modeling (see Comparison with present predator-prey model section) provide evidence that the basic physical mechanism triggering the *L–H* transition is reasonably well captured by the Kim-Diamond model.[16] However, we explicitly point out that other routes to the *L–H* transition may also exist.

SUMMARY AND CONCLUSION

In summary, the energies of as well as the energy transfer between low frequency shear flows and the ambient turbulence has been estimated during the *L–H* transition for the first time. In an *L–H* transition that does not exhibit an *I*-phase (as in Refs. 17 and 21), a transient increase in the zonal flow and turbulent stress are observed showing the important role of zonal flows in the *L–H* transition. When the rate of energy transfer from the turbulence into the zonal flow becomes comparable to the power input into the turbulent kinetic energy, then the turbulence amplitude collapses. The turbulent transport then drops, resulting in a decrease in the fueling of the open field line region. As a result, the D_α signal in the divertor drops. Based on earlier results, it can

then be expected that the edge pressure gradients build up, resulting in the formation of a growing radial electric field just inside the LCFS which then sustains the turbulence suppression via the $E \times B$ shearing mechanism. As a result, the system is driven into the *H*-mode. The results reported here thus indicate that the strong turbulent suppression associated with this energy transfer from the turbulence into the zonal flow acts to trigger the *L–H* transition.

ACKNOWLEDGMENTS

This work was supported by the National Magnetic Confinement Fusion Science Program of China under Contracts Nos. 2011GB107001 and 2010GB104001, the National Natural Science Foundation of China under Contracts Nos. 11075181, 10725523, 10721505, 10990212 as well by the U.S. Department of Energy (DOE) through Grant No. DE-SC0001961 and by the WCI Program of the National Research Foundation of Korea funded by the Ministry of Education, Science and Technology of Korea [WCI 2009-001]. The authors would like to acknowledge the facilities, organizing Committee, and participants of the Festival de Theorie, Aix en Provence, 2011 for stimulating discussions.

[1]R. B. Alley, J. Marotzke, W. D. Nordhaus, J. T. Overpeck, D. M. Peteet, R. A. Pielke, R. T. Pierrehumbert, P. B. Rhines, T. F. Stocker, L. D. Talley *et al.*, Science **299**, 2005 (2003).
[2]R. J. Groebner, K. H. Burrell, and R. P. Seraydarian, Phys. Rev. Lett. **64**, 3015 (1990).
[3]R. A. Moyer *et al.*, Phys. Plasmas **2**, 2397 (1995).
[4]P. H. Diamond, S.-I. Itoh, K. Itoh, and T. S. Hahm, Plasma Phys. Controlled Fusion **47**, R35 (2005).
[5]A. Fujisawa, Nucl. Fusion **49**, 013001 (2009).
[6]G. S. Xu, B. N. Wan, M. Song, and J. Li, Phys. Rev. Lett. **91**, 125001 (2003).
[7]A. Fujisawa *et al.*, Phys. Rev. Lett. **93**, 165002 (2004).
[8]H. Xia and M. G. Shats, Phys. Plasmas **11**, 561 (2004).
[9]C. Holland, G. R. Tynan, R. J. Fonck, G. R. McKee, J. Candy, and R. E. Waltz, Phys. Plasmas **14**, 056112 (2007).
[10]A. Fujisawa *et al.*, Plasma Phys. Controlled Fusion **48**, A365 (2006).
[11]A. D. Liu, T. Lan, C. X. Yu, H. L. Zhao, L. W. Yan, W. Y. Hong, J. Q. Dong, K. J. Zhao, J. Qian, J. Cheng *et al.*, Phys. Rev. Lett. **103**, 095002 (2009).
[12]P. Manz, M. Ramisch, and U. Stroth, Phys. Rev. Lett. **103**, 165004 (2009).
[13]M. Xu, G. R. Tynan, P. H. Diamond, S. H. Müller, C. Holland, J. H. Yu, and Z. Yan, Phys. Rev. Lett. **107**, 055003 (2011).
[14]T. Happel, T. Estrada, E. Blanco, C. Hidalgo, G. D. Conway, U. Stroth, and TJ-II Team, Phys. Plasmas **18**, 102302 (2011).
[15]P. H. Diamond, Y. M. Liang, B. A. Carreras, and P. W. Terry, Phys. Rev. Lett. **72**, 2565 (1994).
[16]E. Kim and P. H. Diamond, Phys. Rev. Lett. **90**, 185006 (2003).
[17]G. D. Conway, C. Angioni, F. Ryter, P. Sauter, and J. Vicente, Phys. Rev. Lett. **106**, 065001 (2011).
[18]T. Estrada, T. Happel, C. Hidalgo, E. Ascasibar, and E. Blanco, Europhys. Lett. **92**, 35001 (2010).
[19]P. Manz, M. Ramisch, and U. Stroth, Phys. Rev. E **82**, 056403 (2010).
[20]G. S. Xu, B. N. Wan, H. Q. Wang, H. Y. Guo, H. L. Zhao, A. D. Liu, V. Naulin, P. H. Diamond, G. R. Tynan, M. Xu *et al.*, Phys. Rev. Lett. **107**, 125001 (2011).
[21]L. Schmitz, L. Zeng, T. L. Rhodes, J. C. Hillesheim, E. J. Doyle, R. J. Groebner, W. A. Peebles, K. H. Burrell, and G. Wang, Phys. Rev. Lett. **108**, 155002 (2012).
[22]K. Miki, P. H. Diamond, O. D. Gurcan, G. R. Tynan, T. Estrada, L. Schmitz, and G. S. Xu, Phys. Plasmas (submitted).
[23]R. A. Moyer, G. R. Tynan, C. Holland, and M. J. Burin, Phys. Rev. Lett. **87**, 135001 (2001).
[24]B. Gonçalves, C. Hidalgo, M. A. Pedrosa, R. O. Orozco, E. Sànchez, and C. Silva, Phys. Rev. Lett. **96**, 145001 (2006).
[25]P. Manz, M. Xu, F. Fedorczak, S. C. Thakur, and G. R. Tynan, Phys. Plasmas **19**, 012309 (2012).
[26]G. Xu, B. Wan, J. Li, X. Gong, J. Hu, J. Shan, H. Li, D. Mansfield, D. Humphreys, V. Naulin *et al.*, Nucl. Fusion **51**, 072001 (2011).
[27]W. Zhang, J. F. Chang, B. N. Wan, G. S. Xu, C. J. Xiao, B. Li, C. S. Xu, N. Yan, L. Wang, S. C. Liu *et al.*, Rev. Sci. Instrum. **81**, 113501 (2010).
[28]K. H. Burrell, T. N. Carlstrom, S. Coda, E. J. Doyle, P. Gohil, R. J. Groebner, J. Kim, R. A. Moyer, W. A. Peebles, C. L. Rettig *et al.*, Plasma Phys. Controlled Fusion **38**, 1313 (1996).
[29]Y. H. Xu, C. X. Xu, J. R. Luo, J. S. Mao, B. H. Liu, J. G. Li, B. N. Wan, and Y. X. Wan, Phys. Rev. Lett. **84**, 3867 (2000).